

Photon-native Quantum Perceptrons and Neural Networks

Md Shadnan Azwad Khan^{†,§}, and Daphné Wang[†]

[†] Algorithms and Applications Team, Quandela, Massy, France

[§] Faculty of Science and Engineering, Sorbonne Université, Paris, France

Email: shadnan.azwad@proton.me



Abstract

Photonic quantum neural networks promise fast, low-energy learning but must reconcile linear optics with nonlinear activations. We present a spiking-inspired, photon-native architecture in the discrete-variable regime, in which reconfigurable interferometers implement learned linear maps and photon detection with classical feedforward yields a broad class of effective nonlinear responses. We first realize a photon-native quantum perceptron that implements decision boundaries beyond those of classical perceptrons. Building on this unit, we construct layered networks that pass a single classical scalar readout between units, the average detection rate, without requiring long-lived quantum memories. Across standard benchmarks, these networks train reliably and achieve accuracies comparable to classical fully connected feedforward neural networks of similar depth and parameter count.

From Neurons to Quantum Perceptrons

A classical perceptron scores inputs with a weighted sum and then applies a nonlinearity. Spiking neurons echo this idea in time: they accumulate events, cross a threshold, and reset—still a “sum-then-activate” computation on average. A *quantum* perceptron keeps the same intuition but changes the substrate: classical data and trainable parameters are encoded into quantum states, a programmable quantum process mixes them, and measurement provides the effective nonlinearity. The readout yields classical signals (e.g., class probabilities or expectation values), and intermediate outcomes can be used for adaptive updates or simple feed-forward, giving a flexible, learning-ready unit that mirrors the perceptron’s role while leveraging quantum feature spaces.

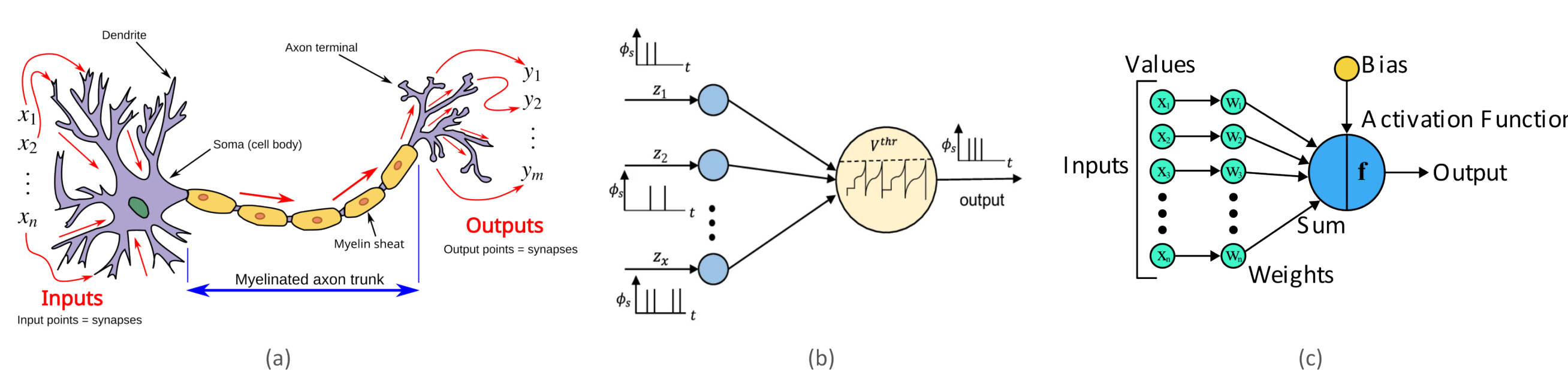


Figure 1: From realistic neuronal models to abstractions: (a) biological neuron [1]; (b) spiking neuron [2]; (c) perceptron.

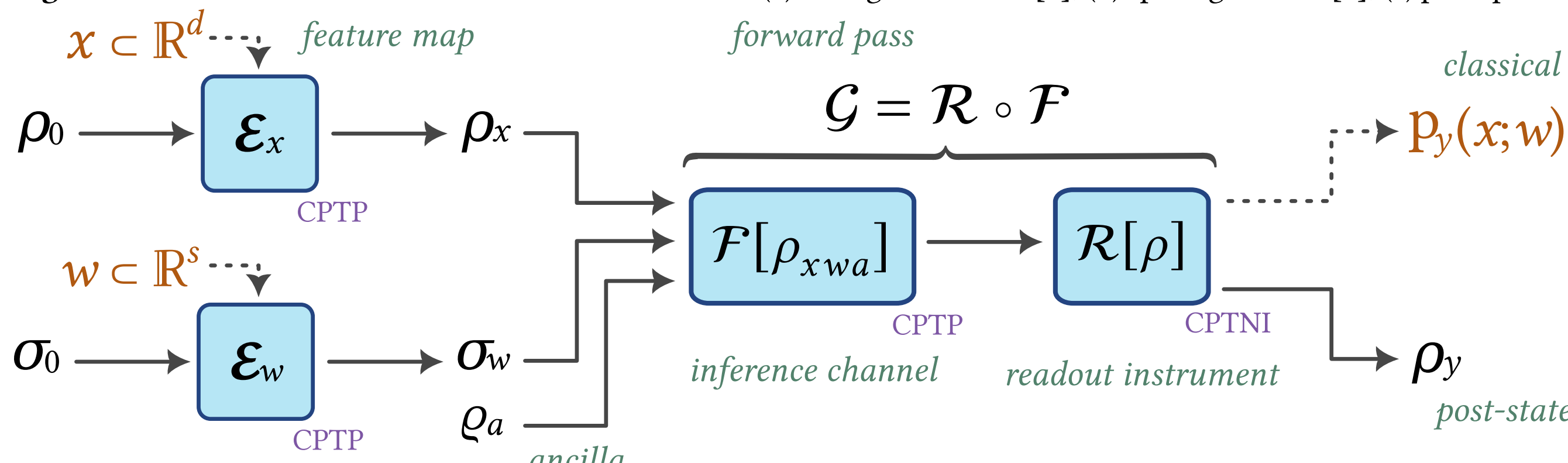


Figure 2: Quantum perceptron schematic. Classical inputs ($x \in \mathbb{R}^d$) and weights ($w \in \mathbb{R}^s$) are embedded by maps ($\mathcal{E}_x, \mathcal{E}_w$) into states (ρ_x, σ_w). Together with ancilla they enter the inference channel ($\mathcal{F}[\rho_{xwa}]$); the readout instrument ($\mathcal{R}[\rho]$) produces classical label probabilities ($p_y(x; w)$) and a post-measurement state (ρ_y). Solid arrows denote quantum flow; dashed arrows denote classical flow. Blue boxes indicate maps; black symbols denote states; purple tags mark CPTP/CPTNI.

Photon-native Neural Computing

Each photonic node behaves like a spiking unit: spatial occupation plays the role of a rate code, multi-photon interference plus photon counting supply the nonlinearity, and the number of shots trades statistical certainty for throughput; layers can be parallelized across devices or serialized on one, with quantum processing inside nodes and only lightweight classical summaries passed between them.

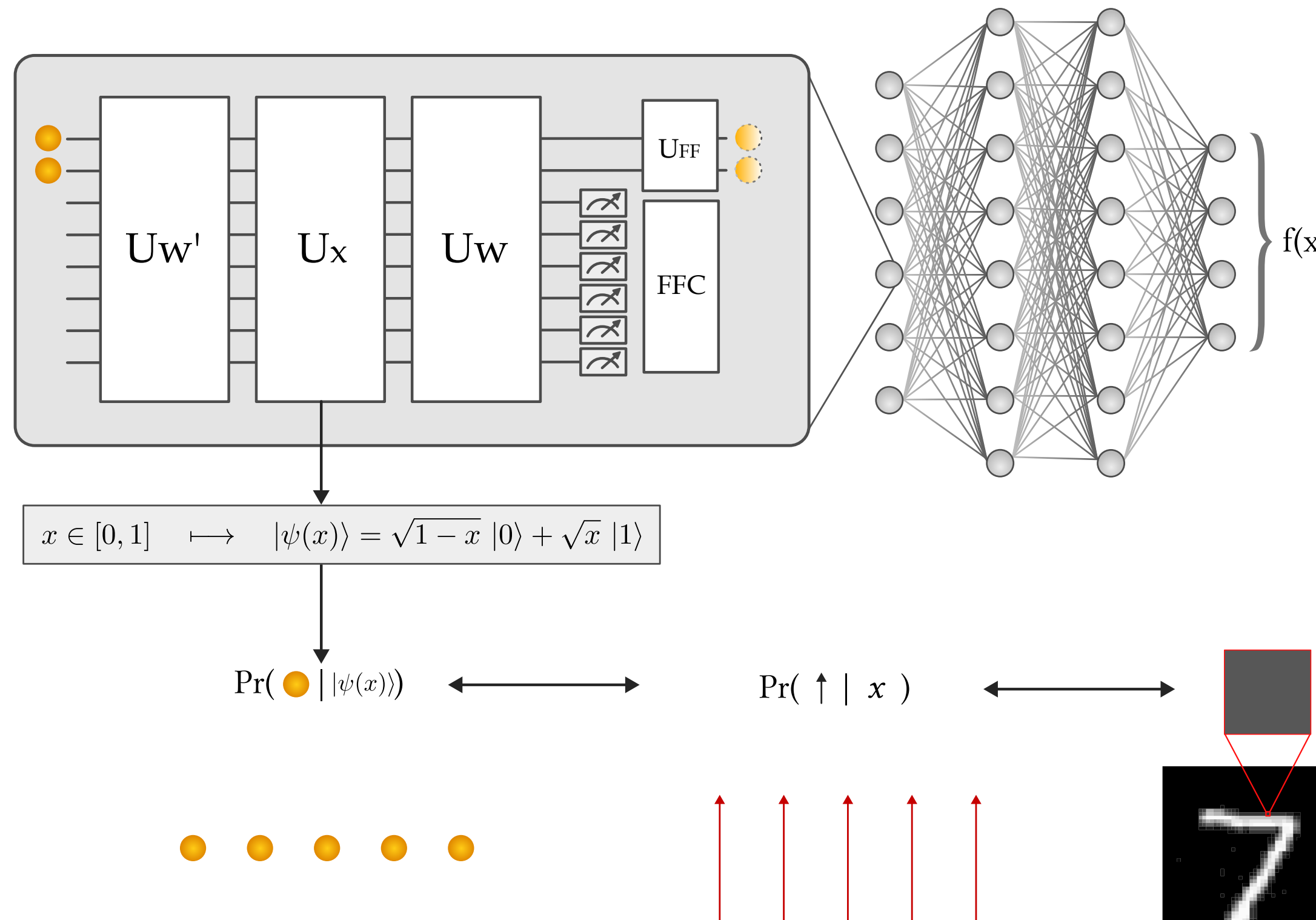


Figure 3: Photon-native quantum neural network with classical communication. Each node is a photon-native quantum perceptron executed in terminal mode; outputs are shot-averaged mean photon counts.

Experimental Results

Summary. On 2D benchmarks the photon-native quantum perceptron learns expressive, nonlinear boundaries (solving XOR) and reaches accuracy on par with the strongest light-weight classical baselines; its performance persists under realistic device noise, and an ablation without the first trainable block remains close to ideal—evidence that the encoder supplies a helpful inductive bias. In image classification with photon-native layers (PnQNN), size-matched models learn faster on MNIST and slightly surpass a compact MLP on CIFAR-10, whereas parameter-matched comparisons favor the wider MLP in peak accuracy and speed; across regimes, PnQNNs often yield better-calibrated probabilities.

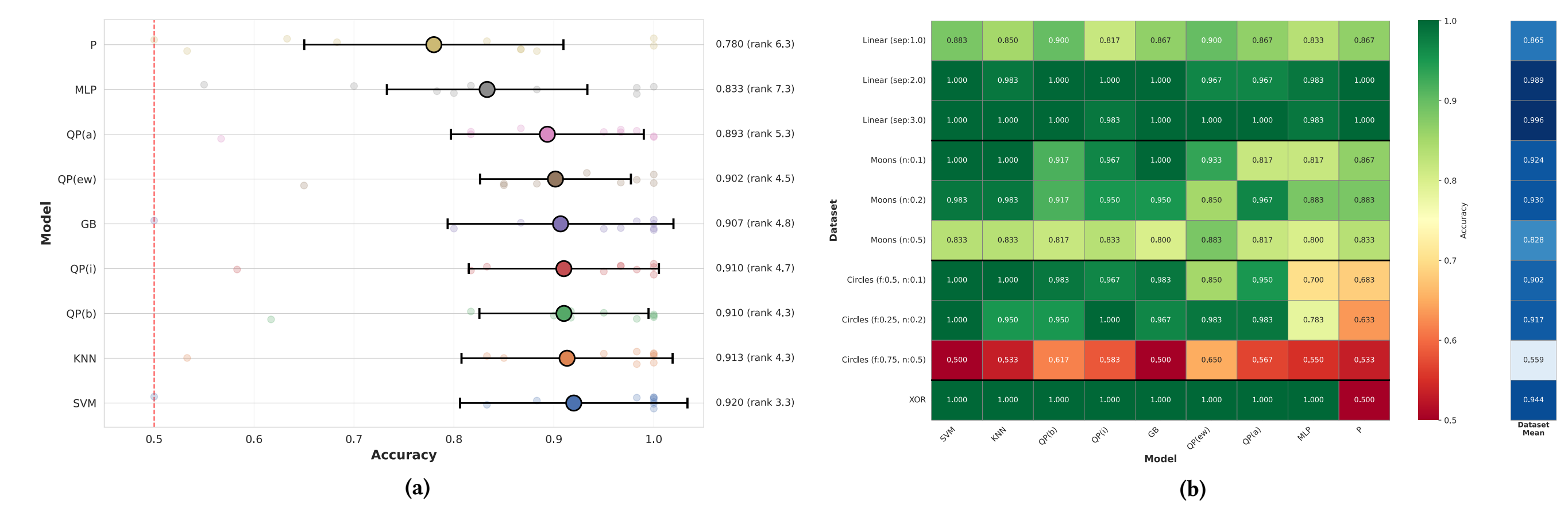


Figure 4: Quantum perceptron (QP) vs. classical baselines. (a) Aggregate performance with confidence intervals. (b) Accuracy by dataset and model (SVM, KNN, GB, perceptron, MLP, QP variants: (i) ideal, (a) Ascella, (b) Belenos, and (ew) encoder-weight ablation without first trainable block).

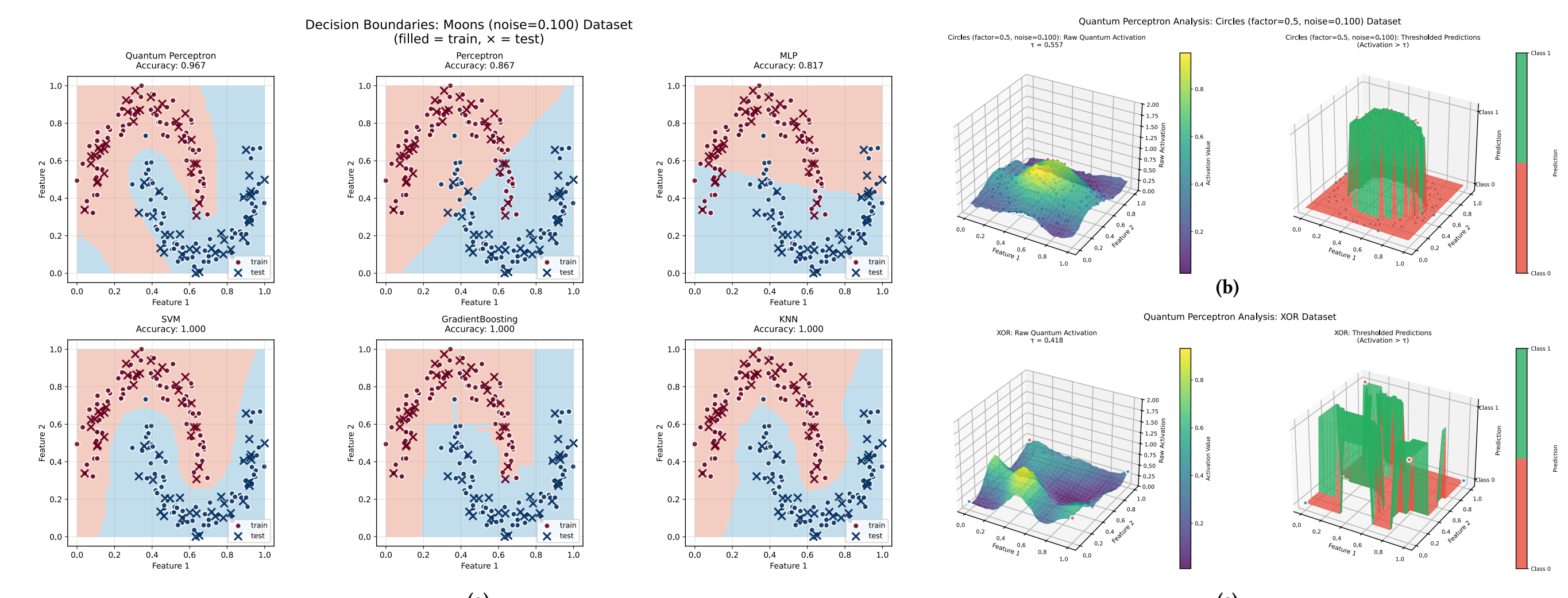


Figure 5: Example PnQP (ideal) outputs: (a) Decision boundary on Moons (noise 0.1) compared with classical baselines; (b) activation surface on Circles (factor 0.5, noise 0.1); (c) activation surface on XOR.

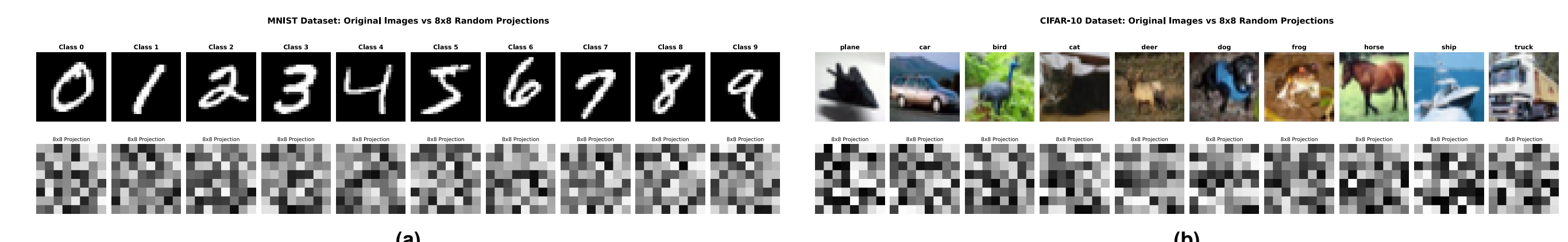


Figure 6: Projected 64-D features after the same fixed random linear map: (a) MNIST and (b) CIFAR-10 (both reshaped 8x8 for display).

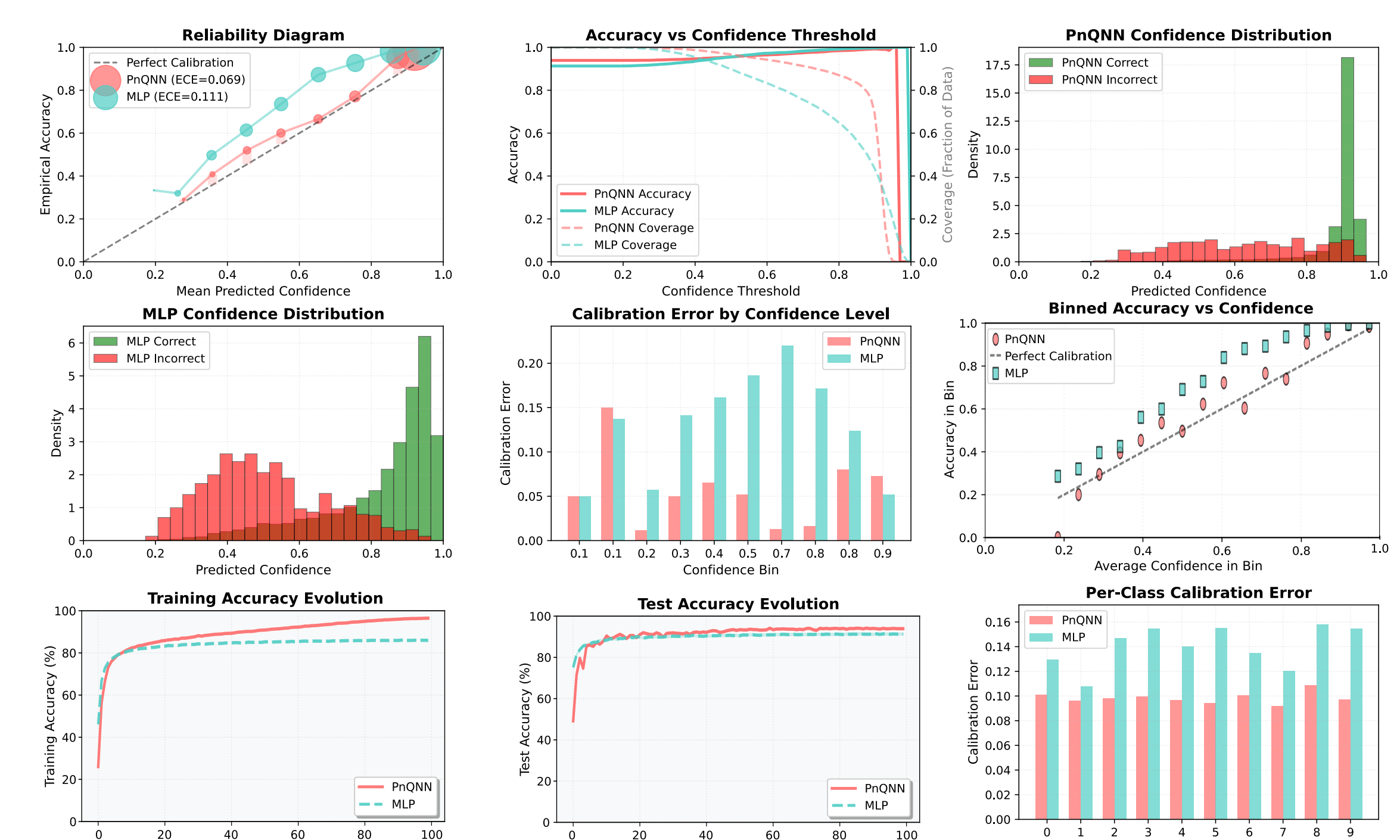


Figure 7: Reliability, calibration, and accuracy metrics (MNIST size-matched).

Dataset	MNIST				CIFAR-10			
	Benchmark	Size-matched	Parameter-matched	Size-matched	Parameter-matched	Size-matched	Parameter-matched	Size-matched
Metric	PhQNN	MLP	PhQNN	MLP	PhQNN	MLP	PhQNN	MLP
Total Parameters	450,174	4,714	118,054	152,330	450,174	4,714	118,054	152,330
Network Architecture	64→32→32→32→10	64→32→32→32→10	64→32→12→12→10	64→256→256→256→10	64→32→32→32→10	64→32→32→32→10	64→32→32→32→10	64→256→256→256→10
Training Time (s)	5,029,23	289,06	1,945,82	347,99	3,187,29	148,28	1,563,32	319,70
Final Train Acc (%)	96.48	85.95	86.58	100.00	49.77	39.41	39.25	98.62
Best Test Acc (%)	94.19	91.48	91.13	95.59	40.19	38.82	38.36	39.56
Final Test Loss	0.6524	0.7550	0.7203	0.6328	1.8668	1.8477	1.8383	2,7047
ECE ↓	0.0609	0.1113	0.0859	0.1035	0.0600	0.0118	0.0127	0.3003
MCE ↓	0.0799	0.2198	0.1695	0.2092	0.1031	0.0249	0.0966	0.4302
Brier Score ↓	0.0980	0.1508	0.1441	0.0837	0.7522	0.7460	0.7476	0.9414
Mean Confidence	0.8703	0.8017	0.8229	0.8519	0.4457	0.3808	0.3750	0.6053
Std Confidence	0.1168	0.1629	0.1542	0.1460	0.1720	0.1490	0.1416	0.2090

Figure 8: PnQNN vs. MLP: consolidated metrics. Side-by-side comparison on MNIST and CIFAR-10 under two regimes—size-matched and parameter-matched. Reported are total parameters, architectures, wall-clock training time, final/train and best/test accuracy, final test loss, and calibration metrics (ECE, MCE, Brier; lower is better), along with mean and standard deviation of predictive confidence.

Conclusion

Capacity is gated by width: each photon-native unit emits one scalar, yet these units already match compact MLPs while often yielding better-calibrated probabilities. Our results are conservative *lower bounds*, taken under a terminal-readout surrogate without inter-node coherence or selective post-selection. Near-term gains: raise feature rank via multi-output photonic blocks and structured/low-rank meshes, and stabilize learning with hardware-in-the-loop shot-aware training.

References

- [1] Loc Vu-Quoc. Neuron and myelinated axon (neuron3.png). Wikimedia Commons, September 2018. URL <https://commons.wikimedia.org/w/index.php?curid=72816083>. CC BY-SA 4.0. Accessed 2025-08-31.
- [2] Marcus Stoffel and Saurabh Balkrishna Tandale. Spiking neural networks for nonlinear regression of complex transient signals on sustainable neuromorphic processors. *npj Unconventional Computing*, 1(1):2, 2024.
- [3] Alexia Salavarros, Nicolas Maring, Pierre-Emmanuel Emeriau, and Shane Mansfield. Photon-native quantum algorithms. *Materials for Quantum Technology*, 5(2):023001, 2025.
- [4] Nicolas Heurtel, Andreas Fyrillas, Grégoire De Gliniasty, Raphaël Le Bihan, Sébastien Malherbe, Marceau Pailhas, Eric Bertasi, Boris Bourdoncle, Pierre-Emmanuel Emeriau, Rawad Mezher, et al. Perceval: A software platform for discrete variable photonic quantum computing. *Quantum*, 7:931, 2023.